PIXEL REDRAWN FOR A ROBUST ADVERSARIAL DEFENSE

Anonymous authors
Paper under double-blind review

ABSTRACT

Recently, an adversarial example becomes a serious problem to be aware of because it can fool trained neural networks easily. To prevent the issue, many researchers have proposed several defense techniques such as adversarial training, input transformation, stochastic activation pruning, etc. In this paper, we propose a novel defense technique, Pixel Redrawn (PR) method, which redraws every pixel of training images to convert them into distorted images. The motivation for our PR method is from the observation that the adversarial attacks have redrawn some pixels of the original image with the known parameters of the trained neural network. Mimicking these attacks, our PR method redraws the image without any knowledge of the trained neural network. This method can be similar to the adversarial training method but our PR method can be used to prevent future attacks. Experimental results on several benchmark datasets indicate our PR method not only relieves the over-fitting issue when we train neural networks with a large number of epochs, but it also boosts the robustness of the neural network.

1 INTRODUCTION

Deep neural networks have exhibited very accurate results, but, are also vulnerable to adversarial examples (Szegedy et al., 2013). Adversarial example is a generated output that induces a trained machine to misclassify a test datum with a high probability. In other words, the adversarial example can fool the trained machine to fail its task (Dhillon et al., 2018b; Goodfellow et al., 2014; Szegedy et al., 2013). We call the method that generates adversarial examples as an attack technique. For instance, in image classification, an attack technique is creating an adversarial image by perturbing some pixels of the original image in which the adversarial image is remained to be perceptible by the human. Obviously, the lesser the pixels to be perturbed, the better the attack technique it is. Defense techniques to prevent those attacks usually need to produce a robust neural network model which can detect adversarial examples or label the adversarial examples correctly. There are many researchers who have studied both attacking and defense techniques, and it is generally believed that the defense techniques are more challenging than the attack techniques.

In this paper, we focus on the defense technique that generates a robust neural network. For this purpose, we have to understand the fundamental idea of generating the adversarial example. In image classification, usually, an adversarial image is generated by perturbing its pixels' value (for example, L_2 or L_∞ attack). If we regard the perturbed pixels to be formed by adding some noises, then the technique of creating the noises can be recognized as a dropout (Srivastava et al., 2014) (if the perturbed pixel value is zero) or other regularization techniques (Adeli & Wu, 1998; Krogh & Hertz, 1992; Nowlan & Hinton, 1992). The neural network with the regularization method usually shows higher performance than the one without the regularization method (normal testing). From another viewpoint, we can regard adversarial examples as a subset from the training dataset universe. Due to the difficulty of collecting all possible examples in the world, we usually just use the clean (unperturbed) examples (Kurakin et al., 2016; Yuan et al., 2017) as the representative of our training dataset.

In order to solve the problem, we propose Pixel Redrawn (PR) method, which is a pre-processing method that redraws a pixel value of the original image into a different pixel value. The PR method is motivated by two observations. The first observation is based on the lesson provided by Carlini and Wagner in (Carlini & Wagner, 2017), which the randomization can increase the distortion required

for attack. The paper has mentioned that the most effective defense technique so far is the dropout randomization which has increased nearly five times more difficulty in generating the adversarial examples on CIFAR dataset. We agree that the randomization method makes it difficult to compute the derivation during the back-propagation and it could replace the perturbed pixel with another value by some random chances during the feed-forward.

The second observation is that humans usually can recognize images regardless of the colors in which the image has been drawn (e.g. in various colors or in gray level). This indicates that we usually (human) may not need to have a colorful image just for image classification. We discuss this in more detail with our proposed method in Section 2.

In this study, we focus on the following:

- We analyze the influence of our PR method toward a normal deep neural network without any adversarial machine learning.
- We evaluate the effectiveness of our PR method applied in the deep neural network against the adversarial example.
- And, we compare our PR method with a random noise injection.

Our research contributions can be summarized as follows:

- Our PR method effectively generates adversarial training images that are not covered in the original dataset.
- Hence, our PR method increases the robustness in neural network training.

To promote reproducible research, we release the implementation of our defense. [1]

2 Pixel Redrawn Method

2.1 Preliminaries

Let X be the image for the input of neural networks. If the size of the image is $m \times n$, then $\{x_i | x_i \in X\}$, where x_i= $x_1, x_2, \ldots, x_{m \times n}$ is the pixel of the image. A classifier $F(\cdot)$ is a function to produce a predicted label $\widehat{Y}$ for X. Let Y be the true label of image X.

An attack technique $A(\cdot)$ is a function to generate an adversarial image X^{adv} from X with (or without) the knowledge of $F(\cdot)$.

2.2 Our Approach

As aforementioned, PR is a pre-processing method $PR(\cdot)$ which reproduces a new image by re-drawing the pixels of the original image. We called the generated image as PR image X^{pr}. We list the three main steps of PR method as follows:

1. **Discretization** Let C be the range of color $C \in [0, 255]$. Note that we use a normalized pixel value $C \in [0, 1]$ in the experiment section (Section 4). If we discretize the color into k sets, then $\{c_i | c_i \in C\}$, where $c_i = c_1, c_2, \ldots, c_k$ is the sub-range of color in C. For each c_i, the range starts from a minimum value $s^{pr}_{i_{min}}$ and ends with a maximum value $s^{pr}_{i_{max}}$ (e.g. $c_1 = [s^{pr}_{1_{min}}, s^{pr}_{1_{max}}] = [0, 51]$ if $k = 5$ and C is equally divided).
2. **Prediction** We train a PR model (describe more in Section 2.3) and then we use it to predict each pixel of an image.
$$\hat{y}^{pr}_i = wx_i + b \tag{1}$$
where $\hat{y}^{pr}_i$ is a prediction label of a pixel from PR model, w is a weight of PR model, x_i is a pixel of an image, and b is a bias of PR model (shown in 'PR process' of Fig. 1).

[1] We modify and extend the scripts from CleverHans. Our scripts are available at https://github.com/canboy123/pixel-redrawn

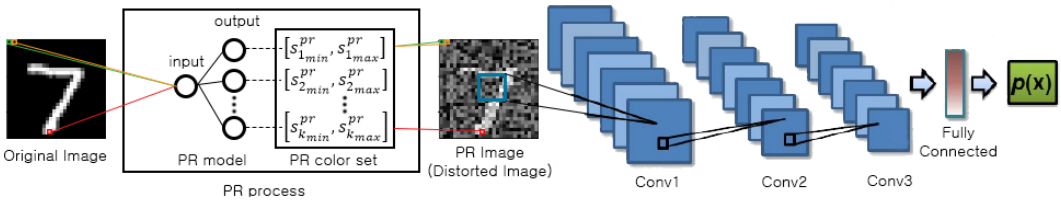

Figure 1: Pixel Redrawn concept with MNIST example.

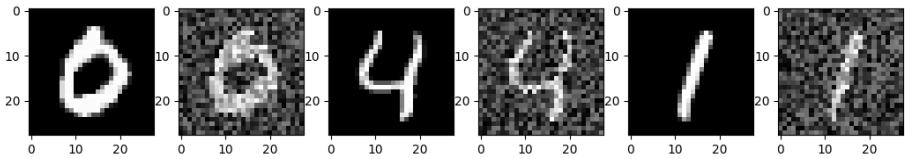

Figure 2: Example of original images and PR images from MNIST dataset. From a pair of an image, the left-hand side is the original image and the right-hand side is the PR image.

3. **Mapping** We redraw the pixel with the sub-range of color c_i that has predicted from PR model.

$$c_i = colorset(y_i^{pr}) \tag{2}$$

$$x_i^{pr} = random_{c_i}(s^{pr}_{i_{min}}, s^{pr}_{i_{max}}) \tag{3}$$

where $colorset(\cdot)$ is the color set that has defined by the user, c_i is the sub-range of color with a minimum value $s^{pr}_{i_{min}}$ and a maximum value $s^{pr}_{i_{max}}$, and $random_{c_i}(\cdot)$ is a random function that generates a random value between $s^{pr}_{i_{min}}$ and $s^{pr}_{i_{max}}$.

In Fig. 1, we perform pre-processing (PR process) for the original image. We reassign each pixel of the image to a random value, such that the range of the random value is based on the chosen sub-range of color which is predicted from PR model. The newly generated PR image is then fed into a neural network.

We depict some examples from a real dataset (i.e. MNIST (LeCun et al., 1998) dataset) with PR method in Fig. 2. The intuition of redrawing each pixel with a certain value in an accepted interval is that, for a certain training image, the training dataset does not include all possible combination of the training image with human-acceptably varying pixel values. With the PR method, we try to include those missing data in the training phase. Another advantage of using the PR method is that we can generate more accurate neural network models (discussed in more detail in Section 2.5). In the following sub-sections, we explain PR model for effectively generating new pixel redrawn images by our PR method.

2.3 Generating Pixel Redrawn Model

Given a pixel value from the original training image x_i, PR model predicts the output pixel value $\hat{y}_i^{pr}$, perturbed within an accepted range c_i, for the corresponding pixel location of the new image x_i^{pr}. Since we redraw each pixel of the image (either grayscale or color) independently which the pixel is the only input for the PR model, and we need the PR model to produce several outputs, then single-layer Perceptron is qualified in this case. Firstly, we train the PR model by generating a batch of random examples with the corresponding labels initialized with the c_i. After the PR model is converged, we predict each pixel of the original image with the newly trained PR model. Lastly, we assign a predicted output value of the winning node at the last layer in the trained PR model to the corresponding pixel location of the new image. Note that the output value is within the accepted range which is initialized by the user. The final output should look similar as the right-hand side image of a pair image in Fig. 2).

2.4 PSEUDO-CODE OF THE PIXEL REDRAWN METHOD

In order to have a clear description of our proposed method, we provide the pseudo-code of the PR method in Algorithm 1. First, we initialize the settings of the PR models, which include the range of each color value c_i, the number of the input (always 1) and output (k), the number of the epochs/iterations, and some random weights. Then, we train the PR model by generating some random inputs with a corresponding label which the label is based on the range of each color value. After we train the PR model, we generate a PR image (X^{pr}) by using the trained PR model to redraw all pixels of the original image (X). Next, we use the newly generated PR image (X^{pr}) as the input of the neural network during the training phase and testing phase. In the end, the trained network show the output label of the test data.

Algorithm 1 The pseudo-code of the Pixel Redrawn Method

Input: Image dataset.
Initialize k, c_i where $c_i = c_1, \ldots, c_k$, random weights
Preprocessing phase:
Train a PR model with a batch of random generated values which has assigned with a proper label
Predict each pixel of the original image (training and test data) with the trained PR model
Generate a PR image X^{pr} by assigning a new pixel value for each pixel of the original image which is based on the output of the trained PR model
Training phase:
Train a neural network with X^{pr}
Testing phase:
Classify X^{pr} with the trained neural network
Output: The class label of the test image

2.5 EXTENSION OF THE PIXEL REDRAWN MODEL

One direct extension is using multiple PR models. We train *d* PR models and predict each pixel of the original image with one of the trained PR models. In other words, we randomly select one PR model out of *d* PR models to predict a pixel of the original image. Then, we repeat the same steps until all pixels are redrawn.

Another extension is partially converged PR models (less accurate) to redraw a pixel to a totally different color value. The partially converged PR model is generated when we prematurely stop the training phase on purpose after a few epochs so that the model is not fully trained. For example, if a black and white (k = 2) PR model has 70% accuracy to predict a pixel either black or white color, then a black color pixel can have 30% chance to be converted into a white color. Note that this may or may not influence the content of the image depending on the number of the pixels that are different from the original input. In the extreme case, PR method may able to change an eye color from black to blue for example, by using the partially converged PR models. The motivation of using the partially converged PR models is because the adversarial example changes a pixel value into a different value which the changed value is far from the original value (L_∞ attack).

In summary, using several PR models (including some partially converged PR models) increase the robustness of the neural network.

3 EXPERIMENTAL SETTINGS

3.1 DATASET

For experimental analysis of our propose methods, we use three public benchmark datasets in this study. The datasets include MNIST, Fashion MNIST (Xiao et al., 2017) and CIFAR-10 (Krizhevsky et al., 2010). For the CIFAR-10 dataset, we generate another grayscale CIFAR-10 for the purpose of analyzing the influence of our proposed method on the color image. MNIST and Fashion MNIST have 60,000 training images and 10,000 test images associated with a label from ten classes. The size of each image is 28×28 grayscale. CIFAR-10, however, has 50,000 training images and 10,000 test images with ten classes. Each image is 32×32 color image.

We use a basic convolutional neural network (CNN) (Krizhevsky et al., 2012) as the neural network architecture for all datasets. The neural network architecture is shown in Fig. 1. We use three convolutional layers and one fully connected layer. The convolutional layers are followed by the Rectifier Linear Unit (ReLU) activation function. The fully connected layer is followed by the Softmax activation function.

3.2 ATTACK TECHNIQUE

There are two kinds of attacks, which are white-box attack and black-box attack. In the white-box attack, attackers know all parameters of the attacked model, whereas in the black-box attack, attackers have no knowledge about the parameters of the attacked model. In this experiment, we run the white-box attack because it is the hardest to defend. The attack can be targeted attack or untargeted attack. In the targeted attack, the attacker tries to deceive the trained network to misclassify the datum as the targeted label. The untargeted attack, on the other hand, is fooling the trained model to misclassify the datum as any label except the true label. We choose the untargeted attack in the experiment because it is easier for the attacker than the targeted attack.

We use several state-of-the-art attack techniques for the evaluation of our proposed method. The attack techniques include Fast Gradient Sign Method (FGSM) (Goodfellow et al., 2014), basic iterative method (BIM) (Kurakin et al., 2016), momentum iterative method (MIM) (Dong et al., 2018) and L_2-Carlini & Wagner's (L_2-CW) (Carlini & Wagner, 2016) attack. During the experiments, when we apply with the FGSM, BIM, and MIM attacks, we set $\epsilon = 0.3$ for the MNIST dataset and $\epsilon = \frac{8}{256}$ for the Fashion MNIST and CIFAR-10 datasets . For CW attack, we set 1,000 in the number of iterations to run the attack.

FGSM It is a fast and simple attack technique to generate the adversarial example which has proposed by Goodfellow et al. (2014). We set this technique as the baseline of attack techniques. The equation of FGSM is computed by

$$X^{adv} = X + \epsilon \; sign(\nabla_X L(X, y)) \tag{4}$$

where ϵ is the maximum perturbation allowed for each pixel and $L(X, y)$ is a loss function.

BIM It is an extension of FGSM by applying multiple iterations with small step size in order to obtain the least perturbations of the image. This technique is proposed by Kurakin et al. (2016). The computation of the technique is shown in Eq. 5

$$X_0^{adv} = X, \; X_{N+1}^{adv} = Clip_{X,\epsilon}\{X_N^{adv} + \alpha \; sign(\nabla_X L(X_N^{adv}, y))\} \tag{5}$$

where $Clip_{X,\epsilon}$ is a function to clip the output image to be within the ϵ-ball of X.

MIM It is more advanced than BIM with momentum algorithm. This technique is proposed by Dong et al. (2018). The computation of the technique is shown in Eq. 6

$$X_{t+1}^{adv} = X_t^{adv} + \alpha \cdot \frac{g_{t+1}}{||g_{t+1}||_2} \tag{6}$$

where g_{t+1} is shown in Eq. 7.

$$g_{t+1} = \mu \cdot g_t + \frac{J(x_t^{adv}, y)}{||\nabla_x J(x_t^{adv}, y)||_1} \tag{7}$$

CW It is an efficient attack technique in finding the adversarial example with the smallest perturbations. The equation is shown as follow.

$$minimize \parallel \frac{1}{2}(tanh(w) + 1) - x \parallel_2^2 + c \cdot f(\frac{1}{2}(tanh(w) + 1)) \tag{8}$$

3.3 DEFENSE TECHNIQUE

We categorize the defense techniques into two different categories. They are white-box defense and black-box defense. In the white-box defense, defenders use only the known attack techniques to generate adversarial examples to be included in a training dataset (e.g. adversarial training (Goodfellow et al., 2014; Madry et al., 2017; Tramèr et al., 2017)). In the black-box defense, on the other

hand, defenders have no knowledge about the attack techniques and they try to generate a robust neural network model (e.g. stochastic activation pruning (SAP) (Dhillon et al., 2018a), input transformations (Guo et al., 2018), etc.). The white-box defense is usually performed better than the black-box defense because it can use the state-of-the-art attack technique to create adversarial examples for the training purpose and then the trained model can prevent the attacks with the similar level (or weaker levels) of the known attack technique. However, unlike the black-box defense, the white-box defense might not be able to defend strong attacks devised in the future. Due to the disability of the white-box defense in defending future attacks, the black-box defense is more reliable to be studied. Therefore, most state-of-the-art defense techniques are the black-box defense.

3.4 Case Study with Different Attack Scenarios

In this paper, we evaluate our method in several cases with different attack scenarios. The case studies are included as follows:

- **Normal:** No attack technique is used. Test the neural networks with a legitimate datum. $\widehat{Y} = F(PR(X))$
- **Case A:** The attackers have no knowledge of the PR method but they knows the parameters of the trained neural networks. The attackers create an adversarial image from an image with the parameters of the trained neural networks. The defense mechanism receives the adversarial image as the input for the PR model and then generate PR image for the input of the trained neural networks.
  $\widehat{Y} = F(PR(A(F, X)))$
- **Case B:** No PR method is used during the testing phase. The attackers have no knowledge of PR method but they knows the parameters of the trained neural networks. The attackers generate an adversarial image from an image with the parameters of the trained neural networks. The trained neural networks use the adversarial image as the input without being pre-processed by the PR method.
  $\widehat{Y} = F(A(F, X))$
- **Case C:** The attackers know both the PR method and the trained neural networks. The attackers produce an adversarial image from an image with the parameters of the PR method and trained neural network. The trained neural networks use the adversarial image as the input without being pre-processed by the PR method.
  $\widehat{Y} = F(A(F, PR, X))$
- **Case D:** The attackers know both the PR method and the trained neural networks. The attackers produce an adversarial image from an image with the parameters of the PR method and trained neural network. The defense mechanism receives the adversarial image as the input for the PR model and the newly created PR image is used as the input of the trained neural networks.
  $\widehat{Y} = F(PR(A(F, PR, X)))$

We illustrate some adversarial images generated from the MNIST dataset for each case in Fig. 3. Note that the adversarial example generated from the case C and D can cause high L_0, L_2 and L_∞ distances because the attacker has used a distorted image instead of a clean image. In other words, the perturbed pixels from the adversarial image can be perceptible by the human.

4 Experimental Results

In this study, we perform several experiments based on the following questions:

1. What is the influence of applying the PR method in different phases with a legitimate test datum?
2. What is the influence of using the PR method in different case studies?
3. What is the difference between multiple PR models and a single PR model applying in the neural networks?
4. What is the difference between the PR method and the random noise injection?

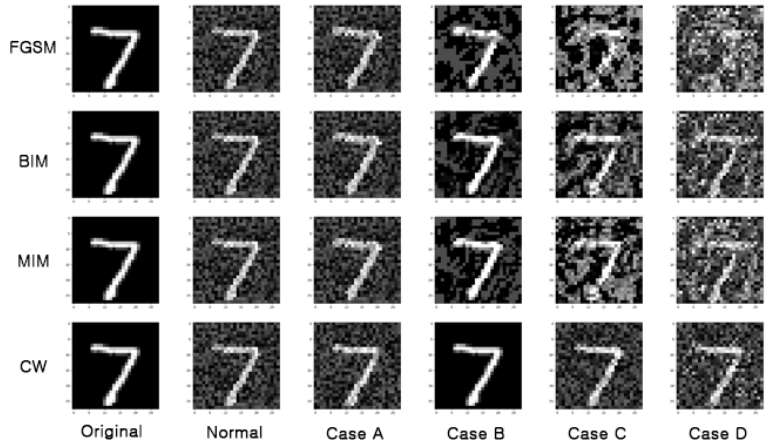

Figure 3: The example of the input images for the classifier from MNIST dataset with FGSM ($\epsilon = 0.3$), BIM ($\epsilon = 0.3$), MIM ($\epsilon = 0.3$), and L_2-CW attack techniques in five cases.

4.1 Experiment to answer Question # 1

The objective of performing these experiments is to demonstrate that PR augmented training method has more advantages than common training methods. From Table 1, we produce four different results by applying the PR method in different phases. These include (1) applying no PR method, denoted as non-PR (i.e. common training method), (2) applying PR method during the training phase, (3) testing phase (4) and both phases. We analyze that applying PR method (either during the training phase or both phases) is not significantly different with non-PR case in terms of the accuracy. This means that neural networks trained with PR method show comparable performance to those trained without PR method. From the results of "Testing Phase" in Table 1, it can be seen that neural networks trained without PR (i.e. non-PR) are not sufficiently robust when they are exposed to images perturbed by PR method. In other words, we can use PR method as an attack technique to fool the trained neural networks. The accuracy for the MNIST and Fashion MNIST datasets are greatly decreased in Table 1 could be caused by over-fitting when a large number of epochs have passed. However, our method can relieve the over-fitting issue as shown in Table 1 when we apply PR method in the training phase only. The neural networks can classify clean images correctly after we train them with PR method. We conjecture PR method has performed regularization while training the neural networks. Common regularization methods (e.g. dropout, weight decay, etc.) usually are related with neural networks architecture, but our PR method is applied to the data themselves.

Table 1: Comparison results of applying pixel redrawn method during various phases.

Dataset	Epoch	Accuracy			
		Non-PR	Training Phase	Testing Phase	Both Phases
MNIST	50	0.9921	0.9905	0.8097	0.9893
	500	0.9885	0.9824	0.4964	0.9879
	1000	0.9893	0.9671	0.2765	0.9865
Fashion MNIST	50	0.9106	0.8879	0.3538	0.8724
	500	0.9058	0.8795	0.3018	0.8670
	1000	0.8964	0.8788	0.2550	0.8632
CIFAR-10	50	0.6179	0.5703	0.5144	0.5386
	500	0.5989	0.5557	0.4864	0.5323
	1000	0.5873	0.5495	0.4739	0.5204
CIFAR-10 (grayscale)	50	0.5697	0.5099	0.3764	0.4845
	500	0.5466	0.4864	0.3429	0.4609
	1000	0.5369	0.4761	0.3370	0.4569

4.2 EXPERIMENT TO ANSWER QUESTION # 2

The goal of operating these experiments is to validate whether PR method can be effectively used as a defense technique against the state-of-the-art attack techniques. We conduct five cases that we have discussed in Section 3.4 in this sub-section. From Table 2, PR method can defend most attacks in the case A and D. One interesting observation that we have found in the case B is that the neural networks which have been trained with PR method during the training phase are robust to defend most attacks (except the L_2-CW attack) even if we do not apply PR method during the testing phase. This shows that our PR method boosts the robustness of the neural networks. For the case C, the performance of the neural networks is significantly degraded due to large increase of L_p distance (i.e. the distance between the original image and the adversarial image). As we know, the case C is not practical because the L_p distance has to be as low as possible in order to create an adversarial example. Although the case C is impractical, we still perform the case D to validate our PR method can increase the robustness of the neural network (except MNIST dataset with FGSM technique because of high distortion of the generated adversarial image as shown in Fig. 3). We conjecture our method which can defend the attacks effectively because it has eliminated most adversarial pixels during the pre-processing phase. Furthermore, we can see that our PR method performs better in the grayscale dataset from the comparison between CIFAR-10 and CIFAR-10 (grayscale) dataset.

Table 2: Results for several datasets in the case A, B, C, and D with 1,000 epochs and k=3. Note that in the case A, we classify as $F(PR(A(F, X)))$. In the case B, we classify as $F(A(F, X))$. In the case C, we classify as $F(A(F, PR, X))$. In the case D, we classify as $F(PR(A(F, PR, X)))$.

Dataset	Attack	Accuracy, k=3				
		Normal	Case A	Case B	Case C	Case D
MNIST	FGSM, $\epsilon = 0.300$	0.9870	0.9689	0.8787	0.6396	0.3664
	BIM, $\epsilon = 0.300$		0.9831	0.7930	0.5115	0.7697
	MIM, $\epsilon = 0.300$		0.9680	0.7504	0.4264	0.5209
	L_2-CW		0.9853	0.6621	0.1526	0.9690
Fashion MNIST	FGSM, $\epsilon = 0.031$	0.8632	0.8426	0.7642	0.6887	0.7430
	BIM, $\epsilon = 0.031$		0.8420	0.7271	0.6277	0.7376
	MIM, $\epsilon = 0.031$		0.8340	0.6815	0.5847	0.7137
	L_2-CW		0.8450	0.1048	0.0932	0.8159
CIFAR-10	FGSM, $\epsilon = 0.031$	0.5204	0.3343	0.2265	0.2177	0.2236
	BIM, $\epsilon = 0.031$		0.3554	0.2104	0.2054	0.2216
	MIM, $\epsilon = 0.031$		0.3025	0.1904	0.1913	0.1938
	L_2-CW		0.4667	0.1728	0.1654	0.4156
CIFAR-10 (grayscale)	FGSM, $\epsilon = 0.031$	0.4569	0.3371	0.2217	0.2016	0.2502
	BIM, $\epsilon = 0.031$		0.3487	0.2079	0.1969	0.2633
	MIM, $\epsilon = 0.031$		0.3216	0.1888	0.1854	0.2291
	L_2-CW		0.4290	0.1845	0.1727	0.3868

In addition, we compare the performance between a neural network trained with PR method (during the training phase) and a neural network trained without PR method under four different attacks, shown in Table 3. Note that we do not apply PR method during testing phase for the neural network that has been trained with PR method (case B). From Table 3, neural networks trained with PR method show higher performance than non-PR neural networks except in the normal case. This result indicates our PR method can increase the robustness of the neural network.

4.3 EXPERIMENT TO ANSWER QUESTION # 3

The target of implementing these experiments is to present the benefit of using the multiple PR models rather than the single PR model. As aforementioned, the case C is impractical since the case C will cause high L_p distance. Hence, we do not include case C (and D) in this sub-section. From Table 4, the one with the multiple PR models outperforms the one with a single PR model. In average of the accuracy, the multiple PR models produce 1.86% and 1.16% higher than the single PR model for case A and B respectively. This shows the multiple PR models produce a stronger defense than the single PR model. We leave the experiments for the parameters tuning of multiple PR models in the future.

Table 3: Comparison of using non-PR model and PR model (case B) in several datasets with 1,000 epochs under four different attacks.

Dataset	Model	Accuracy				
		Normal	FGSM	BIM	MIM	L_2-CW
MNIST	Non-PR	**0.9893**	0.1114	0.1005	0.0844	0.1568
	PR (case B), k=3	0.9870	**0.8787**	**0.7930**	**0.7504**	**0.6621**
Fashion MNIST	Non-PR	**0.8964**	0.6308	0.4221	0.2718	0.0680
	PR (case B), k=3	0.8632	**0.7642**	**0.7271**	**0.6815**	**0.1048**
CIFAR-10	Non-PR	**0.5873**	0.1807	0.1819	0.1761	0.1612
	PR (case B), k=3	0.5204	**0.2265**	**0.2104**	**0.1904**	**0.1728**
CIFAR-10 (grayscale)	Non-PR	**0.5369**	0.1816	0.1876	0.1839	0.1670
	PR (case B), k=3	0.4569	**0.2217**	**0.2079**	**0.1888**	**0.1845**

Table 4: The comparison of using a PR model and multiple PR models in several datasets with 1,000 epochs for the case A and B.

Dataset	Attack	Accuracy			
		single PR		multiple PR	
		Case A	Case B	Case A	Case B
MNIST	FGSM, $\epsilon = 0.300$	0.9689	0.8787	**0.9752**	**0.9371**
	BIM, $\epsilon = 0.300$	0.9831	0.7930	**0.9865**	**0.8003**
	MIM, $\epsilon = 0.300$	0.9680	0.7504	**0.9706**	**0.7693**
	L_2-CW	0.9853	**0.6621**	**0.9875**	0.5767
Fashion MNIST	FGSM, $\epsilon = 0.031$	0.8426	0.7642	**0.8564**	**0.8059**
	BIM, $\epsilon = 0.031$	0.8420	0.7271	**0.8555**	**0.7703**
	MIM, $\epsilon = 0.031$	0.8340	0.6815	**0.8501**	**0.7422**
	L_2-CW	0.8450	0.1048	**0.8476**	**0.1615**
CIFAR-10	FGSM, $\epsilon = 0.031$	0.3343	**0.2265**	**0.3630**	0.2181
	BIM, $\epsilon = 0.031$	0.3554	**0.2104**	**0.3859**	0.2040
	MIM, $\epsilon = 0.031$	0.3025	**0.1904**	**0.3353**	0.1853
	L_2-CW	0.4667	**0.1728**	**0.4964**	0.1717
CIFAR-10 (grayscale)	FGSM, $\epsilon = 0.031$	0.3371	0.2217	**0.3655**	**0.2222**
	BIM, $\epsilon = 0.031$	0.3487	0.2079	**0.3812**	**0.2118**
	MIM, $\epsilon = 0.031$	0.3216	0.1888	**0.3532**	**0.1948**
	L_2-CW	0.4290	**0.1845**	**0.4526**	0.1795

4.4 Experiment to answer Question # 4

The aim of conducting these experiments are to distinguish between PR model and random noise injection. Note that the value of the random noise that we used in this sub-section is between -1.0 and 1.0 with the uniform distribution and we clip the value of the pixel between 0.0 and 1.0 (normalized pixel value). We depict several outputs with the use of the PR method and random noise injection in Fig. 4.

Besides that, we show the experiment results for the random noises injection with the legitimate data in Table 5. We use a similar settings in Section 4.1 to only apply the random noises injection during the training phase, testing phase or both phases. We inspect the PR model (from Table 1) has higher performance than the random noises injection (from Table 5) in the case that the method is applied either during the training phase only or both the training and testing phases. Although the random

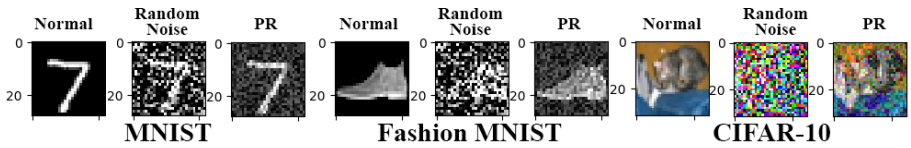

Figure 4: The example of using PR method and some random noises in MNIST, Fashion MNIST and CIFAR-10 datasets. From three images, the left most image is the original image, the middle one is the image after adding some random noises, and the right most image is the PR image.

noise injection has high performance in fooling the trained neural networks (in the case when we apply the random noise injection during the testing phase only), the L_2 distance is larger than our method since the image generated with the random noise injection is not able to be recognized by the human easily (shown in Fig. 4). In summary, the PR method is different from the random noise injection in terms of the performance in maintaining the accuracy when the number of the epoch is increased. Moreover, the PR method also remains the newly generated image perceptible by the human.

Table 5: The comparison results of applying the some random noises on the image during the different phase.

Dataset	Epoch	Accuracy		
		Training Phase	Testing Phase	Both Phases
MNIST	50	0.9871	0.1650	0.9596
	500	0.2789	0.1958	0.9705
	1000	0.1021	0.1695	0.9758
Fashion MNIST	50	0.8275	0.1435	0.8161
	500	0.7308	0.1357	0.8446
	1000	0.7263	0.1297	0.8449
CIFAR-10	50	0.5112	0.2205	0.4779
	500	0.4296	0.1883	0.4674
	1000	0.4194	0.4739	0.4718

4.5 Summary of PR method

From the experiment results, we summarize the contribution of using the PR method as follows:

- The PR method relieves the over-fitting issue by generating different possible output of the image. (Q1)
- The PR method increases the robustness of the neural networks.(Q2)
- The defense level for the one with the multiple PR models is stronger than the one with the single PR model. (Q3)
- The PR model has higher performance than the random noise injection. (Q4)

5 Conclusion

In this study, we propose a novel method, namely Pixel Redrawn method which regenerates the image to all possible forms without compromising human perception. We address four questions in our experiments: **Q1** What is the influence of applying the PR method in different phases with a legitimate test datum?, **Q2** What is the influence of using the PR method in different case studies?, **Q3** What is the difference between multiple PR models and a single PR model applying in the neural networks?, and **Q4** What is the difference between the PR method and the random noise injection? From the experimental results, our method shows that it can prevent the over-fitting problem while maintaining the performance of the neural network, it also improves the robustness of the neural network. Furthermore, our method is more reliable than using some random noises.

References

Hojjat Adeli and Mingyang Wu. Regularization neural network for construction cost estimation. *Journal of construction engineering and management*, 124(1):18–24, 1998.

Nicholas Carlini and David Wagner. Towards evaluating the robustness of neural networks. *arXiv preprint arXiv:1608.04644*, 2016.

Nicholas Carlini and David Wagner. Adversarial examples are not easily detected: Bypassing ten detection methods. In *Proceedings of the 10th ACM Workshop on Artificial Intelligence and Security*, pp. 3–14. ACM, 2017.

Guneet S. Dhillon, Kamyar Azizzadenesheli, Jeremy D. Bernstein, Jean Kossaifi, Aran Khanna, Zachary C. Lipton, and Animashree Anandkumar. Stochastic activation pruning for robust adversarial defense. In *International Conference on Learning Representations*, 2018a. URL https://openreview.net/forum?id=H1uR4GZRZ.

Guneet S Dhillon, Kamyar Azizzadenesheli, Zachary C Lipton, Jeremy Bernstein, Jean Kossaifi, Aran Khanna, and Anima Anandkumar. Stochastic activation pruning for robust adversarial defense. *arXiv preprint arXiv:1803.01442*, 2018b.

Yinpeng Dong, Fangzhou Liao, Tianyu Pang, Hang Su, Jun Zhu, Xiaolin Hu, and Jianguo Li. Boosting adversarial attacks with momentum. *arXiv preprint*, 2018.

Ian J Goodfellow, Jonathon Shlens, and Christian Szegedy. Explaining and harnessing adversarial examples. *arXiv preprint arXiv:1412.6572*, 2014.

Chuan Guo, Mayank Rana, Moustapha Cisse, and Laurens van der Maaten. Countering adversarial images using input transformations. In *International Conference on Learning Representations*, 2018. URL https://openreview.net/forum?id=SyJ7ClWCb.

Alex Krizhevsky, Vinod Nair, and Geoffrey Hinton. Cifar-10 (canadian institute for advanced research). *URL http://www. cs. toronto. edu/kriz/cifar. html*, 2010.

Alex Krizhevsky, Ilya Sutskever, and Geoffrey E Hinton. Imagenet classification with deep convolutional neural networks. In *Advances in neural information processing systems*, pp. 1097–1105, 2012.

Anders Krogh and John A Hertz. A simple weight decay can improve generalization. In *Advances in neural information processing systems*, pp. 950–957, 1992.

Alexey Kurakin, Ian Goodfellow, and Samy Bengio. Adversarial examples in the physical world. *arXiv preprint arXiv:1607.02533*, 2016.

Yann LeCun, Léon Bottou, Yoshua Bengio, and Patrick Haffner. Gradient-based learning applied to document recognition. *Proceedings of the IEEE*, 86(11):2278–2324, 1998.

Aleksander Madry, Aleksandar Makelov, Ludwig Schmidt, Dimitris Tsipras, and Adrian Vladu. Towards deep learning models resistant to adversarial attacks. *arXiv preprint arXiv:1706.06083*, 2017.

Steven J Nowlan and Geoffrey E Hinton. Simplifying neural networks by soft weight-sharing. *Neural computation*, 4(4):473–493, 1992.

Nitish Srivastava, Geoffrey Hinton, Alex Krizhevsky, Ilya Sutskever, and Ruslan Salakhutdinov. Dropout: a simple way to prevent neural networks from overfitting. *The Journal of Machine Learning Research*, 15(1):1929–1958, 2014.

Christian Szegedy, Wojciech Zaremba, Ilya Sutskever, Joan Bruna, Dumitru Erhan, Ian Goodfellow, and Rob Fergus. Intriguing properties of neural networks. *arXiv preprint arXiv:1312.6199*, 2013.

Florian Tramèr, Alexey Kurakin, Nicolas Papernot, Ian Goodfellow, Dan Boneh, and Patrick McDaniel. Ensemble adversarial training: Attacks and defenses. *arXiv preprint arXiv:1705.07204*, 2017.

Han Xiao, Kashif Rasul, and Roland Vollgraf. Fashion-mnist: a novel image dataset for benchmarking machine learning algorithms. *arXiv preprint arXiv:1708.07747*, 2017.

Xiaoyong Yuan, Pan He, Qile Zhu, Rajendra Rana Bhat, and Xiaolin Li. Adversarial examples: Attacks and defenses for deep learning. *arXiv preprint arXiv:1712.07107*, 2017.

A APPENDIX

A.1 EXPERIMENTS TO ANSWER QUESTION #2

In this appendix, we provide Table 6, which is the extended version of Table 2 in Section 4.2. Note that more results with 50 and 500 epochs are added. We also provide Table 7 and 8 with $k = 4$ and $k = 10$ respectively. The purpose of the experiments is to analyze the influence of the k value to the performance of the neural network. From Table 6, 7 and 8, we observe that the bigger the k, the higher the accuracy when we test with the legitimate example, the lower the accuracy when we test with the adversarial examples. In other words, we have to do a trade-off between the legitimate example and adversarial example. Although we believe that multiple PR models could increase the accuracy of the adversarial example while using a large value of k, we leave these experiments in the future.

A.2 EXPERIMENTS TO ANSWER QUESTION #3

In this appendix, we show Table 10 as the extended version of Table 4 in Section 4.3 with the results of the multiple PR models and the single model with two epochs (i.e. 500 and 1,000 epochs).

A.3 EXPERIMENTS TO ANSWER QUESTION #4

In this appendix, we show the comparison results between PR method (case A) and adversarial training with 1,000 epochs for several datasets in Table 11. We apply MIM attack technique during the adversarial training. In Table 11, our method outperforms adversarial training in most cases.

Table 6: Results for several datasets in the case A, B, C, and D with 50, 500, and 1000 epochs and k=3. Note that in the case A, we classify as $F(PR(A(F, X)))$. In the case B, we classify as $F(A(F, X))$. In the case C, we classify as $F(A(F, PR, X))$. In the case D, we classify as $F(PR(A(F, PR, X)))$.

Dataset	Attack	Epoch	Accuracy, k=3				
			Normal	Case A	Case B	Case C	Case D
MNIST	FGSM, $\epsilon = 0.300$	50	0.9897	0.9570	0.8527	0.4187	0.3413
		500	0.9867	0.9698	0.9045	0.5870	0.3919
		1000	0.9870	0.9689	0.8787	0.6396	0.3664
	BIM, $\epsilon = 0.300$	50	0.9897	0.9601	0.4485	0.0260	0.2230
		500	0.9867	0.9786	0.8003	0.3982	0.7223
		1000	0.9870	0.9831	0.7930	0.5115	0.7697
	MIM, $\epsilon = 0.300$	50	0.9897	0.9450	0.3651	0.0119	0.1043
		500	0.9867	0.9636	0.7574	0.3272	0.4788
		1000	0.9870	0.9680	0.7504	0.3956	0.5209
	L_2-CW	50	0.9897	0.9824	0.1617	0.0079	0.9666
		500	0.9867	0.9842	0.6758	0.0837	0.9724
		1000	0.9870	0.9853	0.6621	0.1526	0.9690
Fashion MNIST	FGSM, $\epsilon = 0.031$	50	0.8724	0.8291	0.7366	0.6001	0.6811
		500	0.8670	0.8380	0.7492	0.6748	0.7376
		1000	0.8632	0.8426	0.7642	0.6887	0.7430
	BIM, $\epsilon = 0.031$	50	0.8724	0.8215	0.6944	0.4886	0.6578
		500	0.8670	0.8360	0.7038	0.5899	0.7229
		1000	0.8632	0.8420	0.7271	0.6277	0.7376
	MIM, $\epsilon = 0.031$	50	0.8724	0.8186	0.6662	0.4510	0.6312
		500	0.8670	0.8302	0.6644	0.5484	0.6998
		1000	0.8632	0.8340	0.6815	0.5847	0.7137
	L_2-CW	50	0.8724	0.8292	0.0770	0.0888	0.8170
		500	0.8670	0.8444	0.0826	0.0826	0.8196
		1000	0.8632	0.8450	0.1048	0.0932	0.8159
CIFAR-10	FGSM, $\epsilon = 0.031$	50	0.5386	0.2968	0.1931	0.1893	0.2103
		500	0.5323	0.3256	0.2053	0.2001	0.2186
		1000	0.5204	0.3343	0.2265	0.2155	0.2236
	BIM, $\epsilon = 0.031$	50	0.5386	0.3127	0.1876	0.1865	0.2038
		500	0.5323	0.3385	0.1932	0.1957	0.2114
		1000	0.5204	0.3554	0.2104	0.2054	0.2216
	MIM, $\epsilon = 0.031$	50	0.5386	0.2772	0.1783	0.1815	0.1920
		500	0.5323	0.2898	0.1775	0.1839	0.1916
		1000	0.5204	0.3025	0.1904	0.1913	0.1938
	L_2-CW	50	0.5386	0.4728	0.1646	0.1687	0.4256
		500	0.5323	0.4708	0.1626	0.1765	0.4234
		1000	0.5204	0.4667	0.1728	0.1654	0.4156
CIFAR-10 (grayscale)	FGSM, $\epsilon = 0.031$	50	0.4845	0.3430	0.2216	0.2002	0.2285
		500	0.4609	0.3357	0.2098	0.1960	0.2472
		1000	0.4569	0.3371	0.2217	0.2016	0.2502
	BIM, $\epsilon = 0.031$	50	0.4845	0.3518	0.2112	0.1910	0.2387
		500	0.4609	0.3494	0.2005	0.1924	0.2531
		1000	0.4569	0.3451	0.2079	0.1895	0.2633
	MIM, $\epsilon = 0.031$	50	0.4845	0.3270	0.1971	0.1851	0.2165
		500	0.4609	0.3181	0.1834	0.1819	0.2289
		1000	0.4569	0.3158	0.1888	0.1808	0.2291
	L_2-CW	50	0.4845	0.4424	0.1817	0.1788	0.3865
		500	0.4609	0.4363	0.1727	0.1719	0.3945
		1000	0.4569	0.4290	0.1845	0.1727	0.3868

Table 7: Results for several datasets in the case A, B, C, and D with 50, 500, and 1000 epochs and k=4. Note that in the case A, we classify as $F(PR(A(F, X)))$. In the case B, we classify as $F(A(F, X))$. In the case C, we classify as $F(A(F, PR, X))$. In the case D, we classify as $F(PR(A(F, PR, X)))$.

Dataset	Attack	Epoch	Accuracy, k=4				
			Normal	Case A	Case B	Case C	Case D
MNIST	FGSM, $\epsilon = 0.300$	50	0.9932	0.7421	0.7908	0.5384	0.5502
		500	0.9891	0.8596	0.8756	0.8131	0.8238
		1000	0.9908	0.8114	0.8409	0.7198	0.6961
	BIM, $\epsilon = 0.300$	50	0.9932	0.5126	0.3372	0.0810	0.1680
		500	0.9891	0.9144	0.7817	0.6947	0.8227
		1000	0.9908	0.9283	0.6446	0.4903	0.7386
	MIM, $\epsilon = 0.300$	50	0.9932	0.3238	0.2487	0.0517	0.0978
		500	0.9891	0.7932	0.7231	0.6441	0.7019
		1000	0.9908	0.6979	0.5380	0.3920	0.4730
	L_2-CW	50	0.9932	0.9885	0.2584	0.0471	0.9914
		500	0.9891	0.9881	0.8142	0.7988	0.9892
		1000	0.9908	0.9902	0.8437	0.8034	0.9906
Fashion MNIST	FGSM, $\epsilon = 0.031$	50	0.8896	0.8132	0.7363	0.6531	0.7836
		500	0.8841	0.8450	0.8071	0.7671	0.8220
		1000	0.8830	0.8507	0.8212	0.7761	0.8242
	BIM, $\epsilon = 0.031$	50	0.8896	0.7864	0.6371	0.5140	0.7626
		500	0.8841	0.8330	0.7419	0.6536	0.8170
		1000	0.8830	0.8463	0.7913	0.7207	0.8248
	MIM, $\epsilon = 0.031$	50	0.8896	0.7792	0.6253	0.4984	0.7477
		500	0.8841	0.8280	0.7232	0.6277	0.8070
		1000	0.8830	0.8419	0.7622	0.6811	0.8020
	L_2-CW	50	0.8896	0.8424	0.0739	0.0746	0.8759
		500	0.8841	0.8430	0.1345	0.1217	0.8677
		1000	0.8830	0.8501	0.1590	0.1650	0.8668
CIFAR-10	FGSM, $\epsilon = 0.031$	50	0.5969	0.2398	0.1889	0.1902	0.2038
		500	0.5838	0.2667	0.2020	0.1983	0.2199
		1000	0.5764	0.2809	0.2254	0.2132	0.2391
	BIM, $\epsilon = 0.031$	50	0.5969	0.2397	0.1820	0.1881	0.1993
		500	0.5838	0.2682	0.1916	0.1904	0.2078
		1000	0.5764	0.2887	0.2072	0.1985	0.2253
	MIM, $\epsilon = 0.031$	50	0.5969	0.2126	0.1760	0.1828	0.1890
		500	0.5838	0.2203	0.1755	0.1789	0.1857
		1000	0.5764	0.2347	0.1851	0.1812	0.1961
	L_2-CW	50	0.5969	0.4758	0.1626	0.1681	0.4661
		500	0.5838	0.4716	0.1645	0.1696	0.4573
		1000	0.5764	0.4668	0.1742	0.1705	0.4595
CIFAR-10 (grayscale)	FGSM, $\epsilon = 0.031$	50	0.5362	0.2805	0.1964	0.1904	0.2344
		500	0.5316	0.3061	0.1999	0.1999	0.2501
		1000	0.5210	0.3076	0.2079	0.2027	0.2588
	BIM, $\epsilon = 0.031$	50	0.5362	0.2860	0.1964	0.1839	0.2435
		500	0.5316	0.3135	0.1999	0.1892	0.2591
		1000	0.5210	0.3191	0.2079	0.1928	0.2663
	MIM, $\epsilon = 0.031$	50	0.5362	0.2571	0.1864	0.1802	0.2218
		500	0.5316	0.2679	0.1830	0.1773	0.2221
		1000	0.5210	0.2719	0.1903	0.1813	0.2238
	L_2-CW	50	0.5362	0.4710	0.1762	0.1672	0.4543
		500	0.5316	0.4642	0.1668	0.1693	0.4557
		1000	0.5210	0.4595	0.1763	0.1680	0.4494

Table 8: Results for several datasets in the case A, B, C, and D with 50, 500, and 1000 epochs and k=10. Note that in the case A, we classify as $F(PR(A(F, X)))$. In the case B, we classify as $F(A(F, X))$. In the case C, we classify as $F(A(F, PR, X))$. In the case D, we classify as $F(PR(A(F, PR, X)))$.

Dataset	Attack	Epoch	Accuracy, k=10				
			Normal	Case A	Case B	Case C	Case D
MNIST	FGSM, $\epsilon = 0.300$	50	0.9933	0.8324	0.6713	0.4700	0.6466
		500	0.9897	0.8754	0.7677	0.7641	0.8184
		1000	0.9890	0.8196	0.7500	0.6874	0.6644
	BIM, $\epsilon = 0.300$	50	0.9933	0.4206	0.1431	0.0681	0.1809
		500	0.9897	0.8125	0.5887	0.5203	0.7374
		1000	0.9890	0.8583	0.5935	0.5968	0.7864
	MIM, $\epsilon = 0.300$	50	0.9933	0.2076	0.0758	0.0333	0.0693
		500	0.9897	0.5491	0.4203	0.3167	0.3952
		1000	0.9890	0.5912	0.4350	0.3323	0.3881
	L_2-CW	50	0.9933	0.9906	0.0877	0.0231	0.9928
		500	0.9897	0.9892	0.8272	0.5395	0.9896
		1000	0.9890	0.9877	0.4854	0.4725	0.9880
Fashion MNIST	FGSM, $\epsilon = 0.031$	50	0.8957	0.7773	0.6876	0.6381	0.7889
		500	0.8864	0.8156	0.7825	0.7558	0.8172
		1000	0.8802	0.8257	0.8029	0.7700	0.8188
	BIM, $\epsilon = 0.031$	50	0.8957	0.7282	0.5497	0.4788	0.7643
		500	0.8864	0.7935	0.7055	0.6570	0.8142
		1000	0.8802	0.8265	0.7712	0.7141	0.8288
	MIM, $\epsilon = 0.031$	50	0.8957	0.7154	0.5449	0.4728	0.7531
		500	0.8864	0.7753	0.6710	0.6124	0.7985
		1000	0.8802	0.8147	0.7241	0.6501	0.8177
	L_2-CW	50	0.8957	0.8369	0.0681	0.0714	0.8854
		500	0.8864	0.8185	0.1400	0.1374	0.8682
		1000	0.8802	0.8282	0.1532	0.1475	0.8633
CIFAR-10	FGSM, $\epsilon = 0.031$	50	0.6087	0.1928	0.1855	0.1808	0.1883
		500	0.5989	0.1945	0.1836	0.1840	0.1936
		1000	0.5918	0.2006	0.1906	0.1903	0.2022
	BIM, $\epsilon = 0.031$	50	0.6087	0.1892	0.1822	0.1795	0.1885
		500	0.5989	0.1901	0.1801	0.1819	0.1951
		1000	0.5918	0.1971	0.1868	0.1828	0.2013
	MIM, $\epsilon = 0.031$	50	0.6087	0.1840	0.1797	0.1766	0.1780
		500	0.5989	0.1766	0.1742	0.1754	0.1815
		1000	0.5918	0.1819	0.1781	0.1763	0.1811
	L_2-CW	50	0.6087	0.3658	0.1591	0.1608	0.3792
		500	0.5989	0.3967	0.1672	0.1678	0.4038
		1000	0.5918	0.3884	0.1665	0.1640	0.4063
CIFAR-10 (grayscale)	FGSM, $\epsilon = 0.031$	50	0.5626	0.1973	0.1895	0.1886	0.1941
		500	0.5566	0.2012	0.1872	0.1834	0.1894
		1000	0.5545	0.2126	0.1949	0.1923	0.2027
	BIM, $\epsilon = 0.031$	50	0.5626	0.1980	0.1857	0.1865	0.1932
		500	0.5566	0.1945	0.1799	0.1800	0.1929
		1000	0.5545	0.2083	0.1869	0.1850	0.1982
	MIM, $\epsilon = 0.031$	50	0.5626	0.1890	0.1813	0.1816	0.1857
		500	0.5566	0.1761	0.1704	0.1733	0.1778
		1000	0.5545	0.1841	0.1757	0.1757	0.1801
	L_2-CW	50	0.5626	0.4075	0.1664	0.1689	0.4189
		500	0.5566	0.4206	0.1594	0.1591	0.4373
		1000	0.5545	0.4247	0.1656	0.1629	0.4336

Table 9: The comparison of using non-PR model and PR model (case B) in several datasets with 50, 500, and 1,000 epochs under four different attacks.

Dataset	Attack	Epoch	Accuracy	
			non-PR	PR (case B), k=3
MNIST	Normal	50	**0.9921**	0.9897
		500	**0.9885**	0.9867
		1000	**0.9893**	0.9870
	FGSM, $\epsilon = 0.300$	50	0.2004	**0.8527**
		500	0.2187	**0.9045**
		1000	0.1114	**0.8787**
	BIM, $\epsilon = 0.300$	50	0.0369	**0.4485**
		500	0.0576	**0.8003**
		1000	0.1005	**0.7930**
	MIM, $\epsilon = 0.300$	50	0.0230	**0.3651**
		500	0.0549	**0.7574**
		1000	0.0844	**0.7504**
	L_2-CW	50	0.0156	**0.1617**
		500	0.1018	**0.6758**
		1000	0.1568	**0.6621**
Fashion MNIST	Normal	50	**0.9106**	0.8724
		500	**0.9058**	0.8670
		1000	**0.8964**	0.8632
	FGSM, $\epsilon = 0.031$	50	0.6083	**0.7366**
		500	0.6624	**0.7492**
		1000	0.6308	**0.7642**
	BIM, $\epsilon = 0.031$	50	0.4265	**0.6944**
		500	0.4064	**0.7038**
		1000	0.4221	**0.7271**
	MIM, $\epsilon = 0.031$	50	0.3566	**0.6662**
		500	0.2401	**0.6644**
		1000	0.2718	**0.6815**
	L_2-CW	50	0.0647	**0.0700**
		500	0.0652	**0.0826**
		1000	0.0680	**0.1048**
CIFAR-10	Normal	50	**0.6179**	0.5386
		500	**0.5989**	0.5323
		1000	**0.5873**	0.5204
	FGSM, $\epsilon = 0.031$	50	0.1801	**0.1931**
		500	0.1753	**0.2053**
		1000	0.1807	**0.2265**
	BIM, $\epsilon = 0.031$	50	0.1767	**0.1876**
		500	0.1751	**0.1932**
		1000	0.1819	**0.2104**
	MIM, $\epsilon = 0.031$	50	0.1741	**0.1783**
		500	0.1723	**0.1775**
		1000	0.1761	**0.1904**
	L_2-CW	50	0.1603	**0.1646**
		500	0.1576	**0.1626**
		1000	0.1612	**0.1728**
CIFAR-10 (grayscale)	Normal	50	**0.5697**	0.4845
		500	**0.5466**	0.4609
		1000	**0.5369**	0.4569
	FGSM, $\epsilon = 0.031$	50	0.1781	**0.2216**
		500	0.1732	**0.2098**
		1000	0.1816	**0.2217**
	BIM, $\epsilon = 0.031$	50	0.1786	**0.2112**
		500	0.1768	**0.2005**
		1000	0.1876	**0.2079**
	MIM, $\epsilon = 0.031$	50	0.1745	**0.1971**
		500	0.1744	**0.1834**
		1000	0.1839	**0.1888**
	L_2-CW	50	0.1597	**0.1817**
		500	0.1621	**0.1727**
		1000	0.1670	**0.1845**

Table 10: The comparison of using a PR model and multiple PR models in several datasets with 500 and 1,000 epochs respectively, for case A and case B.

Dataset	Attack	Epoch	Accuracy			
			single PR		multiple PR	
			Case A	Case B	Case A	Case B
MNIST, $\epsilon = 0.300$	FGSM	500	0.9698	0.9045	**0.9724**	**0.9350**
		1000	0.9698	0.8787	**0.9752**	**0.9371**
	BIM	500	0.9786	0.8003	**0.9816**	**0.8224**
		1000	0.9831	0.7930	**0.9865**	**0.8003**
	MIM	500	0.9636	0.7574	**0.9645**	**0.7806**
		1000	0.9680	0.7504	**0.9706**	**0.7693**
	L_2-CW	500	0.9842	**0.6758**	**0.9872**	0.3273
		1000	0.9853	**0.6621**	**0.9875**	0.5767
Fashion MNIST, $\epsilon = 0.031$	FGSM	500	0.8380	0.7492	**0.8582**	**0.7903**
		1000	0.8426	0.7642	**0.8564**	**0.8059**
	BIM	500	0.8360	0.7038	**0.8527**	**0.7575**
		1000	0.8420	0.7271	**0.8555**	**0.7703**
	MIM	500	0.8302	0.6644	**0.8503**	**0.7310**
		1000	0.8340	0.6815	**0.8501**	**0.7422**
	L_2-CW	500	0.8444	0.0826	**0.8487**	**0.1432**
		1000	0.8450	0.1048	**0.8476**	**0.1615**
CIFAR-10, $\epsilon = 0.031$	FGSM	500	0.3256	0.2053	**0.3470**	**0.2104**
		1000	0.3343	**0.2265**	**0.3630**	0.2181
	BIM	500	0.3385	0.1932	**0.3689**	**0.2013**
		1000	0.3554	**0.2104**	**0.3859**	0.2040
	MIM	500	0.2898	0.1775	**0.3189**	**0.1847**
		1000	0.3025	**0.1904**	**0.3353**	0.1853
	L_2-CW	500	0.4708	0.1626	**0.4947**	**0.1709**
		1000	0.4667	**0.1728**	**0.4964**	0.1717
CIFAR-10 (grayscale), $\epsilon = 0.031$	FGSM	500	0.3357	0.2098	**0.3665**	**0.2174**
		1000	0.3371	0.2217	**0.3655**	**0.2222**
	BIM	500	0.3534	0.2005	**0.3750**	**0.2083**
		1000	0.3487	0.2079	**0.3812**	**0.2118**
	MIM	500	0.3234	0.1834	**0.3526**	**0.1917**
		1000	0.3216	0.1888	**0.3532**	**0.1948**
	L_2-CW	500	0.4363	0.1727	**0.4483**	**0.1829**
		1000	0.4290	**0.1845**	**0.4526**	0.1795

Table 11: The comparison between PR method (case A) and adversarial training in several datasets with 1,000 epochs.

Dataset	Attack	Accuracy	
		PR	Adversarial Training
MNIST, $\epsilon = 0.300$	FGSM	0.9691	**0.9712**
	BIM	**0.9825**	0.9264
	MIM	**0.9672**	0.9287
Fashion MNIST, $\epsilon = 0.031$	FGSM	**0.8503**	0.8408
	BIM	**0.8489**	0.8190
	MIM	**0.8446**	0.8059
CIFAR-10, $\epsilon = 0.031$	FGSM	0.3343	**0.3830**
	BIM	**0.3554**	0.3495
	MIM	0.3025	**0.3072**